

H₂-He vibrational line-shape parameters: Measurement and semiclassical calculation

J. W. Forsman,* J. Bonamy, and D. Robert

Laboratoire de Physique Moléculaire, Université de Franche-Comté, 25030 Besançon-Cedex, France

J. Ph. Berger, R. Saint-Loup, and H. Berger

Laboratoire de Physique, Université de Bourgogne, 21000 Dijon, France

(Received 2 March 1995)

High-resolution inverse Raman spectroscopy has been used to obtain the line shifting and line broadening coefficients of H₂ perturbed by He. Measurements have been made for the *Q*-branch transitions ($J=0$ to 5) in a density range of 10 to 20 amagat and from 296 to 995 K. Up to 795 K we have directly deduced from the experimental broadening coefficients the inelastic rotational state-to-state and vibrational dephasing rates. At higher temperatures, owing to the larger number of channels of relaxation which occur, the results have been analyzed using a scaling law. The line shift and broadening coefficients exhibit a square root and a linear dependence on temperature, respectively, and a significant J dependence. Semiclassical calculations based on an accurate *ab initio* potential lead to line-shape parameters consistent with experiment. They allow a clear understanding of their observed temperature dependence.

PACS number(s): 33.70.Jg

I. INTRODUCTION

Hydrogen is a key molecule for spectroscopic studies of collisional dynamics due to its simplicity allowing pertinent tests of *ab initio* calculations [1]. Its role in diagnostics of combustion processes has led to an extension of measurements of vibrational line-shape parameters in the high-temperature range [2]. Further experimental investigations for H₂ diluted in argon have revealed the important effect of speed-dependent collisional inhomogeneity on these line-shape parameters [3]. Asymmetric features were observed in Raman *Q*-branch transitions as well as a strong deviation from the usual linear mixing rule for the linewidth. As a consequence, the determination of the collisional broadening and shifting parameters from the observed vibrational line profiles required a theoretical model accounting for these speed-dependent collisions [3,4]. Such models include dephasing collisions and collisions changing the speed in the same or in different events. The first observation [3] has prompted new measurements [5] of the *Q*-branch line-shape parameters in a large temperature range for H₂ perturbed by Ne, Ar, and Xe. These three molecular systems exhibit the expected features (i.e., asymmetric profile and nonlinearity of the line broadening versus concentration). These effects are more pronounced the heavier the perturber. For the case of He perturber, the presence of a residual Doppler effect in the considered range of density (between 10 and 20 amagat), which corresponds to the "Dicke regime" [6], needs a specific study to get a clear estimate of the inhomogeneous effect.

The particular interest in the H₂-He system, both for cosmological reasons and for being the simplest prototype of the collisional model, enhances the need for an exhaustive, accurate study of its Raman *Q*-branch line profile. Notice that in spite of these specific motivations, only few data are available [7,8]. The aim of this paper is to perform an exhaustive experimental study of the *Q*-line profiles. In the second section, we report high-resolution measurements of line broadening and shifting coefficients versus concentration for the $J=0$ to 5 *Q*-branch transitions from 296 to 995 K. An accurate analysis of both vibrational and state-to-state rotational transfer rates is given in Sec. III. Section IV is devoted to semiclassical calculation results for the collisional linewidths and line shifts versus temperature and to a comparison with the experimental data. Section V contains a discussion and concluding remarks.

II. EXPERIMENTAL RESULTS

A. Experimental device

Inverse Raman spectroscopy (IRS) was used to observe the *Q*-branch transitions ($J=0$ to 5) and the spectra were recorded with the Raman spectrometer of Dijon University. Since the experiment has been previously described [5], we will emphasize only the differences pertinent to the present study. The measurements were made at densities lying between 10 and 20 amagat, at temperatures from 296 to 995 K, and in a concentration range depending on the population of the probed rotational level. For instance, at 296 K for the *Q*(1) line, we have been able to record spectra in a highly diluted mixture (2% of H₂), but for the *Q*(5) line, we have only been able to observe the Raman signal at concentrations higher than 50% of H₂. The transducer used for the pressure measurements

*Present address: Department of Physics, University of Toronto, Toronto, Ontario, Canada.

was in continuous contact with the gas sample but placed externally to the heater. Thus, the pressure was measured for each spectrum with an accuracy of $\pm 0.3\%$. Gas densities were calculated in amagat units using the virial expression (limited to second order). For the H₂-He mixture, the second virial coefficient is given by

$$\mathcal{B}_T = c_{\text{H}_2}^2 \mathcal{B}_{\text{H}_2\text{-H}_2} + 2c_{\text{H}_2} c_{\text{He}} \mathcal{B}_{\text{H}_2\text{-He}} + c_{\text{He}}^2 \mathcal{B}_{\text{He-He}} \quad (1)$$

The second virial coefficients $\mathcal{B}_{\text{H}_2\text{-H}_2}$ and $\mathcal{B}_{\text{He-He}}$ have been taken from experimental data [9,10] and the interaction virial coefficient $\mathcal{B}_{\text{H}_2\text{-He}}$ has been experimentally determined [11] up to 323 K. At higher temperature we have calculated this coefficient according to Ref. [12]. The magnitude of the largest virial correction to the density was found to be less than 1% whatever the mixture. Temperatures were measured with thermocouples accurate to ± 2.5 K from 295 to 600 K and to $\pm 0.75\%$ of the temperature (expressed in °C) above 600 K. The temperature was monitored with two thermocouples which were not in physical contact with the gas volume. Indeed, the first one was near the heater and the other one was located in a small hole made in the cell and centered on the sample gas volume. With another configuration of the vessel, we measured the real temperature by locating a thermocouple exactly at the center of the gas volume in order to avoid systematic temperature measurement errors. The measurement discrepancies between this thermocouple and the one placed outside the gas volume (in the small hole) were found to be equal to 4 K at 450 and 600 K and equal to 5 K at 800 and 1000 K. The temperature corrections due to these discrepancies were taken in the following. As a consequence of the errors on pressure and temperature, the density error was estimated to be less than 1.5%.

B. Line shift and linewidth measurements

The measurements have been realized in a large temperature range and for highly diluted mixtures. As observed in H₂-X (X = Ne, Ar, and Xe) mixtures [5], a large variation of the line shift with temperature is found for H₂-He, but no unusual features are observed for the line shape: the profile is purely Lorentzian and the broadening coefficient is linear versus He concentration within the experimental uncertainties. Note that the experiments on the H₂-He system have provided the opportuni-

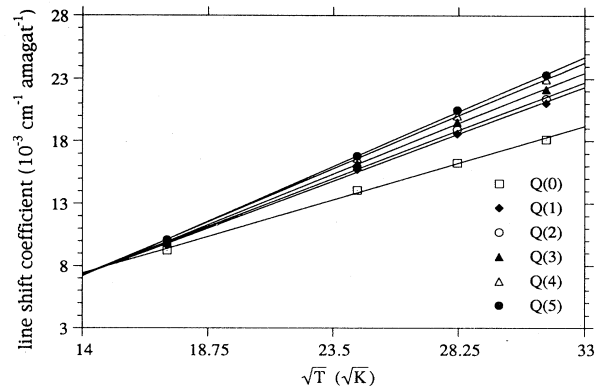


FIG. 1. The line-shift coefficients (symbols) of the Q-branch transitions ($J=0$ to 5) for the H₂-He system versus the square root of the temperature. These data are modeled by straight lines.

ty to measure the line broadening and line-shifting coefficients of pure H₂ in the same conditions and to compare them with previous measurements [2]. Some of the values reported in Ref. [5] have been slightly modified here because the new measurements are more accurate.

1. Collisional line-shift coefficient

Since the line profiles are purely Lorentzian, the center of gravity corresponds to the line peak frequency. Moreover, for the considered range of densities, we have supposed a linear dependence of the frequency shift on the density ($\omega_J = \omega_J^0 + \delta_J \rho$) and we have used the zero-density line positions given by Rahn and Rosasco [2]. Line-shift coefficients of pure H₂ are reported in Table I. At room temperature, our data are in excellent agreement with the previous ones. At high temperature, a discrepancy appears which may result from the temperature measurement as discussed in Refs. [2] and [5]. The usual mixing rule [$\delta = c_A \delta_A + (1 - c_A) \delta_{A-B}$] has been applied to determine the H₂-He collisional shift coefficients (Table II). As it has already been observed in Ref. [5] for the other H₂-rare-gas pairs, the temperature dependence of the line-shift coefficients is well modeled by a square-root temperature law [$\delta_{\text{coll}}(T) = B\sqrt{T} + C$; cf. Fig. 1 and Table III]. Since the B coefficients vary with J , it is clear that the shift exhibits a significant rota-

TABLE I. Experimental collisional line-shift coefficients (expressed in $10^{-3} \text{ cm}^{-1} \text{ amagat}^{-1}$) for pure H₂. Numbers in parentheses indicate the estimated experimental uncertainty.

J	296 K	298 K ^a	295 K ^b	596 K	795 K	995 K	1000 K ^b
0	-2.27(5)	-2.14(17)	-2.10(6)	2.80(7)	5.50(10)	7.90(15)	8.45(18)
1	-3.20(5)	-3.20(3)	-3.20(5)	2.52(10)	5.70(10)	8.30(15)	9.16(11)
2	-1.97(5)		-1.86(6)	3.48(15)	6.45(10)	8.90(15)	9.73(18)
3	-1.95(10)		-1.82(6)	3.23(15)	6.20(15)	8.70(10)	9.65(18)
4	-1.57(10)		-1.52(5)	3.98(15)	6.95(15)	9.60(15)	10.34(18)
5	-1.47(10)		-1.42(6)	4.30(15)	7.00(15)	9.75(15)	10.46(18)

^aReference [13].

^bReference [2].

TABLE II. Experimental line-shift coefficients (in $10^{-3} \text{ cm}^{-1} \text{ amagat}^{-1}$) for the $\text{H}_2\text{-He}$ collisional system. Numbers in parentheses indicate the estimated experimental uncertainty.

J	296 K	RT ^a	RT ^b	596 K	795 K	995 K
0	9.25(20)			14.07(25)	16.26(30)	18.12(40)
1	9.66(10)	11.00(40)	9.4	15.73(15)	18.59(20)	21.04(15)
2	9.76(15)			15.94(25)	18.91(25)	21.39(20)
3	9.91(15)			16.05(20)	19.51(20)	22.15(20)
4	10.10(25)			16.62(35)	20.01(20)	22.97(20)
5	10.10(30)			16.80(35)	20.47(20)	23.33(20)

^aRoom temperature, Ref. [7].

^bRoom temperature, Ref. [8].

tional dependence. The physical mechanisms underlying the J and T dependence of the line shifts will be analyzed in Sec. IV.

2. Collisional broadening coefficient

The experiments have been carried out in the density range from 10 to 20 amagat, thus well above the Dicke minimum [equal to $\approx 2.7, 1.8$ amagat at 295 K and for the $Q(1)$ transition when the perturbers are H_2 and He, respectively] [7,8]. For pure H_2 and for the $\text{H}_2\text{-He}$ mixture, the residual Doppler effect must be accounted for in this ‘‘Dicke regime.’’ The linewidth without Doppler broadening is then given by

$$\Gamma(T) = \Gamma^{\text{obs}}(T) - \frac{2\pi\mathcal{D}\nu_R^2}{c\rho}, \quad (2)$$

where $\Gamma_{(T)}^{\text{obs}}$ is the half-width at half maximum of the observed Lorentzian line shape, c is the speed of light, ν_R is the Raman frequency, and \mathcal{D} is the optical diffusion coefficient. In this expression $\Gamma^{\text{obs}}(T)$ and $\Gamma(T)$ are expressed in $\text{cm}^{-1} \text{ amagat}^{-1}$, ν_R in cm^{-1} , and \mathcal{D} in $\text{cm}^2 \text{ amagat s}^{-1}$. The broadening coefficients γ are defined as $\gamma = \Gamma/\rho$, where ρ is the density in amagat units.

The determination of the collisional line broadening coefficients $\gamma_{\text{coll}}(T)$ from the observed Q -line profile is closely tied to the variation of the experimental Γ_J values versus concentration [5]. As an example, Fig. 2 shows such a variation for the $Q(1)$ line at 296 K. No obvious nonlinearity is observed within the experimental uncer-

tainties. This remains true whatever J and T .

In a first step, the analysis of these data may be done, as usual, by considering that the spectral lines are homogeneous so that $\gamma_{\text{coll}}(T) = \gamma(T)$. The assumed linear dependence of γ_{coll} versus He concentration and the pure H_2 data (Table IV) lead to the $\gamma(T)$ values for $\text{H}_2\text{-He}$ in the limit of an infinitely dilute mixture (Table V). The temperature dependence of these two sets of γ_{coll} are well modeled by a linear law [$\gamma_{\text{coll}}(T) = A'T + C$; cf. Table III].

Of course, even if the difference of mass between He and H_2 is small compared with that of Ne, Ar, or Xe and H_2 , which permits a higher efficiency of the speed-changing collisional mechanism in the narrowing, the question of a residual inhomogeneous contribution in $\gamma(T)$ must be carefully analyzed for the $\text{H}_2\text{-He}$ system. In the RTBT model [4], this inhomogeneity is due to the speed distribution of the shift and the narrowing is induced by the speed changing and dephasing (SCD) collisions. The analysis of the observed $Q(J)$ linewidths [5] for $\text{H}_2\text{-X}$ ($X = \text{Ne, Ar, and Xe}$) using the RTBT model has led to the determination of a characteristic ratio of collision frequencies $x = \nu_{\text{SCD}}/\nu_{\text{tot}}$ ($\nu_{\text{tot}} = \nu_{\text{SCD}} + \nu_D$), where ν_D is the frequency of dephasing collisions which varies only weakly with the perturber mass (0.15, 0.12, and 0.08, respectively, for Ne, Ar, and Xe at room temperature). The homogeneous case corresponds to $x = 1$ [4], so it is realistic to explore the possibility of an x value for $\text{H}_2\text{-He}$ lower than 1 and consistent with the observed concentration dependence of $\gamma(T)$ (cf. Fig. 2).

TABLE III. Parameters B , C , A' , and C' of the expressions $\delta(T) = B\sqrt{T} + C$ and $\gamma(T) = A'T + C'$, fitted through a least-squares procedure to the experimental line shifts and linewidths. B is expressed in $10^{-3} \text{ cm}^{-1} \text{ amagat}^{-1} \text{ K}^{-1/2}$, A' in $10^{-3} \text{ cm}^{-1} \text{ amagat}^{-1} \text{ K}^{-1}$, and C, C' in $10^{-3} \text{ cm}^{-1} \text{ amagat}^{-1}$.

J	0	1	2	3	4	5
$B_{\text{H}_2\text{-H}_2}$	0.707(4)	0.804(5)	0.762(4)	0.741(8)	0.777(3)	0.780(9)
$B_{\text{H}_2\text{-He}}$	0.63(2)	0.80(2)	0.82(2)	0.86(1)	0.90(1)	0.93(2)
$C_{\text{H}_2\text{-H}_2}$	-14.44(4)	-17.04(11)	-15.07(9)	-14.73(19)	-14.96(8)	-14.87(23)
$C_{\text{H}_2\text{-He}}$	-1.52 (44)	-4.05(39)	-4.24(37)	-4.87(25)	-5.33(10)	-5.80(36)
$A'_{\text{H}_2\text{-H}_2}$	9.08(30)	5.00(9)	5.48(17)	3.96(29)	4.25(8)	4.38(9)
$A'_{\text{H}_2\text{-He}}$	11.71(55)	7.16(21)	8.55(13)	8.13(16)	8.16(26)	7.24(27)
$C'_{\text{H}_2\text{-H}_2}$	-1.38(17)	-0.61(5)	-0.20(10)	0.98(17)	0.39(5)	-0.18(6)
$C'_{\text{H}_2\text{-He}}$	-1.63(34)	-0.39(12)	-0.31(9)	-0.23(11)	-0.74(20)	-0.43(21)

TABLE IV. Experimental broadening coefficients $\gamma(T)$ (expressed in $10^{-3} \text{ cm}^{-1} \text{ amagat}^{-1}$) for pure H₂. Numbers in parentheses indicate the estimated experimental uncertainty.

J	296 K	298 K ^a	295 K ^b	596 K	795 K	995 K	1000 K ^b
0	1.30(5)	1.28(1)	1.33(1)	4.00(7)	6.10(10)	7.50(15)	7.60(10)
1	0.87(5)	0.87(1)	0.87(2)	2.21(10)	3.40(10)	4.35(15)	4.28(9)
2	1.45(5)		1.48(1)	2.95(15)	4.20(10)	5.30(15)	5.05(8)
3	2.20(10)		2.21(1)	3.15(15)	4.20(10)	5.00(10)	4.90(8)
4	1.64(10)		1.71(3)	2.95(15)	3.80(15)	4.55(15)	4.50(8)
5	1.10(10)		1.17(3)	2.50(15)	3.30(15)	4.15(15)	4.04(8)

^aReference [13].

^bReference [2].

In a second step, we have thus reanalyzed the $\gamma(T)$ linewidths through the RTBT model with $x < 1$. The residual inhomogeneity would lead to $\gamma_{\text{coll}}(T)$ values lower than those obtained for $x = 1$ (cf. Table V). A maximum value of x ($x_{\text{max}} = 0.5$) consistent within the experimental uncertainties and assumed to be J independent has been determined from the calculated nonlinearity of γ versus the concentration (Fig. 3). Notice that even for $x_{\text{max}} = 0.5$, the calculated line profile does not exhibit any significant asymmetry. The resulting inhomogeneous contributions at room temperature are 0.21, 0.35, 0.42, 0.41, 0.45, and $0.47 \times 10^{-3} \text{ cm}^{-1} \text{ amagat}^{-1}$ for $J = 0$ to 5, respectively. This clearly means that a possible correction to γ_{coll} (cf. Table V), resulting from a residual inhomogeneity, must not be *a priori* discarded. This is particularly true for the higher J values, due to the decrease of γ versus J and the concomitant increase of the above inhomogeneous contributions. This behavior seems realistic since the inhomogeneity tied to the speed distribution of the line shift can be related to the J variation of the shift itself (cf. Fig. 1).

III. RATE LAW ANALYSIS

A. Determination of the vibrational dephasing and rotational inelastic rates up to 795 K

Vibrational dephasing broadening cannot be neglected because rotationally inelastic energy transfers are small

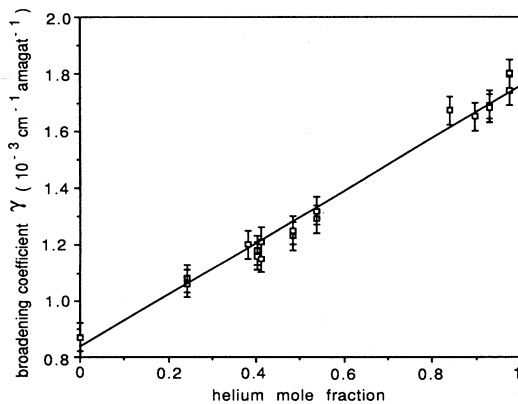


FIG. 2. The experimental broadening coefficients $\gamma(T)$ (expressed in $10^{-3} \text{ cm}^{-1} \text{ amagat}^{-1}$) of the $Q(1)$ line are plotted versus the helium mole fraction at 296 K.

owing to the large value of the rotational constant for H₂, and the absence of an elastic rotational contribution in isotropic Raman scattering [14]. In order to determine the respective contributions of those two kinds of collisions (i.e., elastic vibrational and inelastic rotational) to the line broadening coefficients, we have supposed a J -independent vibrational dephasing contribution (cf. Refs. [2] and [16]). The broadening coefficients may then be expressed as [15]

$$\gamma_{\text{coll}}(J, v) = \gamma_v - \sum_{J' \neq J} W_{J'J}, \quad (3)$$

where γ_v is the vibrational dephasing broadening and $W_{J'J}$ represents the real part of the off-diagonal elements of the rotational relaxation matrix W . The matrix element $-W_{J'J}$ describes the collisional energy transfer rate from rotational level J to level J' and is assumed to be the same in the $v = 0$ and 1 vibrational levels.

To determine each of the two contributions to the broadening, Smyth *et al.* [16] have used a fitting law (exponential gap law) to model the inelastic rotational rates $-W_{J'J}$ and to extract the γ_v value from experimental data through Eq. (3). To avoid the use of such a phenomenological model on which γ_v is dependent, we have determined the inelastic rotational and vibrational dephasing rates directly from the broadening coefficients at 296, 596, and 795 K without making any assumption about the rate law. We have used only Eq. (3) and the detailed balance condition

$$n_J W_{J'J} = n_{J'} W_{JJ'}, \quad (4)$$

where n_J and $n_{J'}$ are the relative populations of molecules in the J and J' rotational levels, respectively. In this tem-

TABLE V. Experimental broadening coefficients $\gamma(T)$ (expressed in $10^{-3} \text{ cm}^{-1} \text{ amagat}^{-1}$) for the H₂-He system. Numbers in parentheses indicate the estimated experimental uncertainty.

J	296 K	596 K	795 K	995 K
0	1.95(20)	5.05(25)	7.64(30)	10.31(40)
1	1.76(10)	3.75(15)	5.26(20)	6.85(20)
2	2.25(15)	4.70(25)	6.42(25)	8.26(20)
3	2.20(15)	4.48(20)	6.15(20)	7.93(20)
4	1.75(25)	3.85(35)	5.75(20)	7.41(20)
5	1.65(30)	3.90(35)	5.46(20)	6.68(20)

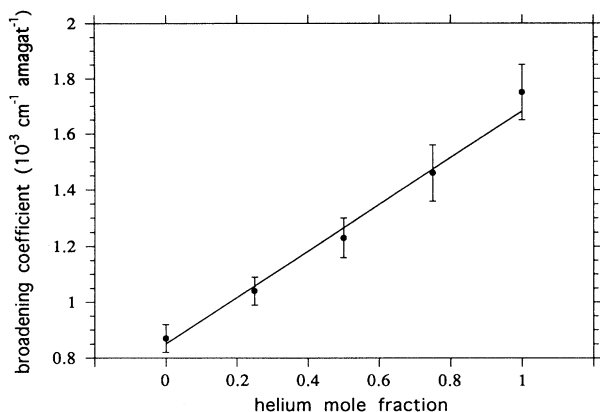


FIG. 3. The calculated broadening coefficients at 296 K obtained with the RTBT model for $x_{\text{He}}=0.5$ and $x_{\text{H}_2}=1$ are plotted versus the helium mole fraction. The error bars correspond to the experimental uncertainties evaluated at this temperature. The straight line is a linear interpolation.

perature range (from 296 to 795 K), we have supposed that the energy-transfer collisions are only significant for the transitions $0 \rightarrow 2$, $1 \rightarrow 3$, $2 \rightarrow 4$, and $3 \rightarrow 5$. Indeed, the rotational energy defects for the $0 \rightarrow 4$ and $4 \rightarrow 6$ transitions are about 1200 and 1320 cm^{-1} , respectively, which is more than twice the translational energy at 800 K ($kT \approx 555 \text{ cm}^{-1}$). Thus, W_{40} and W_{64} can be reasonably neglected. At each of the three temperatures investigated (296, 596, and 795 K), a system of six equations is obtained:

$$\begin{aligned}
 \gamma_{\text{coll}}(0, v) &= \gamma_v - W_{20}, \\
 \gamma_{\text{coll}}(1, v) &= \gamma_v - W_{31}, \\
 \gamma_{\text{coll}}(2, v) &= \gamma_v - (n_0/n_2)W_{20} - W_{42}, \\
 \gamma_{\text{coll}}(3, v) &= \gamma_v - (n_1/n_3)W_{31} - W_{53}, \\
 \gamma_{\text{coll}}(4, v) &= \gamma_v - (n_2/n_4)W_{42}, \\
 \gamma_{\text{coll}}(5, v) &= \gamma_v - (n_3/n_5)W_{53}.
 \end{aligned} \tag{5}$$

The five unknown parameters ($\gamma_v, W_{20}, W_{31}, W_{42}, W_{53}$),

TABLE VI. Rotational transfer ($-W_{J,J}$) and vibrational dephasing (γ_v) rates for the $\text{H}_2\text{-He}$ system, expressed in $10^{-3} \text{ cm}^{-1} \text{ amagat}^{-1}$. Numbers in italics are the rates obtained with the ECS-P model; the others are directly deduced from the broadening coefficients (see the text).

	296 K	596 K	795 K	995 K
$-W_{20}$	0.403(41) <i>0.333</i>	1.97(29) <i>2.02</i>	3.88(40) <i>3.69</i>	<i>5.67</i>
$-W_{31}$	0.071(8) <i>0.05</i>	0.60(16) <i>0.59</i>	1.47(28) <i>1.28</i>	<i>2.21</i>
$-W_{42}$	0.0026(23) <i>0.008</i>	0.188(79) <i>0.223</i>	0.775(15) <i>0.592</i>	<i>1.145</i>
$-W_{53}$	not significant	0.081(35) <i>0.093</i>	0.365(80) <i>0.288</i>	<i>0.628</i>
γ_v	1.68(3)	3.24(23)	3.87(35)	4.95

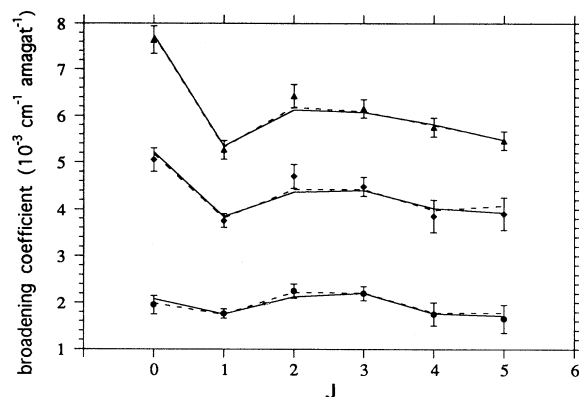


FIG. 4. Comparison at several temperatures (\bullet , 296 K; \blacklozenge , 596 K; \blacktriangle , 795 K) of the experimental broadening coefficients (symbols) (Table V) and the broadening coefficients calculated with the rotational transfer and vibrational dephasing rates. The dotted and solid lines show the results, respectively, with and without an inhomogeneous contribution to the broadening.

determined with a least-squares method from our experimental broadening values, are reported in Table VI. As it is obviously expected, the $-W_{J,J}$ parameters strongly decrease with the rotational defect $\Delta E_{J,J} = |E_{J'} - E_J|$ and increase with temperature. Broadening coefficients calculated with these parameters are in good agreement with the experimental values as shown in Fig. 4. A residual inhomogeneous contribution has also been supposed to determine the five parameters (cf. Sec. II B 2). In this case, the agreement of the calculated broadening with experiment is slightly better (cf. Fig. 4).

At 995 K, the rates W_{40} and W_{64} become significant ($kT \approx 693 \text{ cm}^{-1}$) and since the number of unknown parameters becomes larger than the number of equations, the resolution of the system is no longer possible. Thus, we have followed the procedure proposed by Smyth *et al.* [16]. The rotational parts of the broadening coefficients have been modeled with a dynamical relaxation law to get the best agreement with experiment.

B. Relaxation model

The scaling dynamical relaxation models have proved to describe accurately the rotational transfer rates [17–19]. These scaling laws express all the energy-transfer rates in terms of basis rate constants, i.e., a subset of the W -relaxation matrix (typically a column or a row). Accordingly, the energy-corrected sudden law (ECS), based on the infinite order sudden approximation and accounting for the rotational energy spacing and finite duration of collisions, allows the determination of all the elements of the relaxation matrix through the basis rate constants W_{0L} . The ECS scaling law transition from an initial rotational level J to a final level J' is given by [17]

$$W_{J'J}^{\text{ECS}} = (2J' + 1) \exp[(E_J - E_{J'})/kT] \Omega_{J'}^2 \times \sum_L \begin{bmatrix} J & J' & L \\ 0 & 0 & 0 \end{bmatrix}^2 (2L + 1) \Omega_L^{-2} W_{0L}(T), \quad (6)$$

where $J >$ is the greater of J and J' , L varies between $|J' - J|$ and $J' + J$, the term in large parentheses is a $3-J$ symbol, and $\Omega_{J'}$ and Ω_L are adiabatic factors characterized by a scaling length l_c . To model the basis rate constants for the H₂-He system, the power law (denoted ECS-P) has given the best agreement [19]. The W_{0L} term is modeled by

$$-W_{0L}(T) = \frac{A_0(T/T_0)^N}{[L(L+1)]^\alpha}. \quad (7)$$

The five parameters determined from the broadening coefficients (cf. Table IV) for the four considered temperatures are $A_0 = 197 \times 10^{-3} \text{ cm}^{-1} \text{ amagat}^{-1}$, $N = 1.32 \pm 0.13$, $l_c = 0.55 \pm 0.05 \text{ \AA}$, $\alpha = 3.48 \pm 0.35$, and $\gamma_v(995 \text{ K}) = 4.95 \times 10^{-3} \text{ cm}^{-1} \text{ amagat}^{-1}$ (with a weighted standard deviation $\sigma = 1.08$). For 296, 596, and 795 K, the γ_v values of Table VI have been subtracted from the experimental broadening to get the rotational contribution. Notice that the ECS-P law requires that the variations of one parameter at each iteration be restricted for stability [18]. Because of the large correlation of the parameter A_0 with the others, this parameter has been bounded. The agreement of the resulting fit for the inelastic rotational broadening coefficient versus J is shown in Fig. 5. Note that the corresponding fit for the broadening coefficient accounting for a residual inhomogeneous contribution (cf. Sec. II B 2) leads to a slight improvement.

The rotational energy transfer rates deduced from the procedures described above, as well as the corresponding vibrational dephasing coefficients γ_v , have been gathered in Table VI. The values calculated from the ECS-P model with an allowance for a possible residual inhomogeneity have not been given since the difference between the two sets of data is inside the uncertainties for the rotational rates. They are significant for the dephasing coefficient γ_v (cf. Fig. 6). A direct measurement by laser

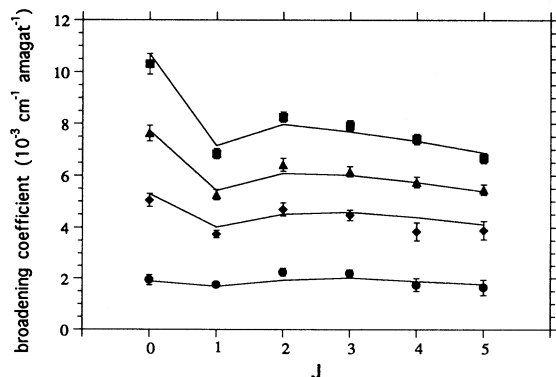


FIG. 5. Comparison at several temperatures (●, 296 K; ◆, 596 K; ▲, 795 K; ■, 995 K) of the experimental broadening coefficients (symbols) and the broadening coefficients predicted by the ECS-P law (solid lines).

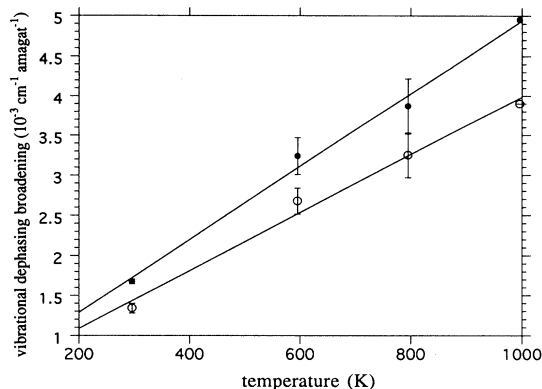


FIG. 6. The vibrational dephasing broadening, determined with (symbols ○) and without (symbols ●) inhomogeneous contribution, are reported versus the temperature. These two sets of data are well modeled by straight lines.

induced fluorescence of the $-W_{31}$ rate is consistent with the present result [$-W_{31} = 0.09(4)$, cf. Ref. [20]]. Furthermore it would be interesting to compare the present γ_v value for H₂-He to that for the other rare-gas perturbers. This would require an exhaustive study of the broadening parameters similar to the present one. In Ref. [5], only the $Q(1)$ line has been investigated.

This analysis clearly shows that the H₂-He rotational broadening coefficients (and the corresponding transfer rates) have been accurately determined in spite of a possible inhomogeneous residual broadening. In contrast, the accuracy of the vibrational broadening coefficient is tied to the magnitude of this inhomogeneity. In the present analysis the inhomogeneous contribution has been maximized (through the parameter $x_{\text{max}} = 0.5$ in the RTBT model; cf. Sec. II B 2) leading to a decrease of the γ_v magnitude by a factor of about 20% but keeping a linear dependence with temperature (Fig. 6). The accurate measurement of this possible inhomogeneous contribution to the broadening could be achieved by using time-resolved nonlinear techniques [21].

IV. SEMICLASSICAL CALCULATIONS OF LINE BROADENING AND LINE SHIFTING COEFFICIENTS

Theoretical line-shape parameters for the Q -branch spectra of the H₂-He system at high temperature were calculated using a semiclassical formalism [22] and an *ab initio* intermolecular potential [23]. The calculations are entirely numeric because the intermolecular potential is not in analytic form. The discussion deals first with the potential and a comparison to other potential surfaces before describing the details of the calculation. A comparison of the theoretical and experimental results concludes this section.

A. Potential-energy surfaces

The H₂-He pair is one of the simplest molecular systems, and the calculation of line-shape parameters can be achieved with available highly accurate intermolecular

potential surfaces. The energy surface in this case is only slightly anisotropic over most of the intermolecular interaction range, and it is necessary to consider elastic and inelastic collisions of H_2 with He. Consequently the potential surfaces must be determined not only for the equilibrium H-H separation, but also for other separations which would permit the consideration of excited vibrational states of H_2 . It will be shown later that the anisotropy of the potential and the dependence of the potential on the vibrational coordinate of the hydrogen molecule contribute significantly to the line-shape parameters. Thus, a suitable potential is described in terms of the collision distance, R , the vibrational coordinate, r , and an angle. A representation convenient for use in the calculation is a series of Legendre polynomials

$$E(R, r, \theta) = \sum_{k=0} V_{2k}(R, r) P_{2k}(\theta), \quad (8)$$

where θ is the angle of the molecular axis relative to the colliding pair. Three accurate potentials were found for H_2 -He and are considered in the following paragraphs.

One of the most accurate *ab initio* potentials available [23] is represented as a set of coefficients, namely V_0 , V_2 , and V_4 , tabulated as functions of r and R . It is a composition of two slightly different potentials [24] as their calculations, based on the CI-type method (where CI denotes configuration interaction), were performed for either the SCF and intrasystem correlations or the intersystem correlation. The final potential is a grid for five intramolecular distances from 0.9 to 2.0 a.u. For the purpose of computing the line-shape parameters, the potential was interpolated with a cubic spline in R and a quadratic function in r in order to have the isotropic potential in the $J=0, v=0$ state ($r=1.449$ a.u.), the difference between the isotropic potential of the $J=0, v=1$ ($r=1.545$

a.u.) and $v=0$ states, and the corresponding quantities for the P_2 part of the anisotropic potential (Fig. 7). We have ignored the P_4 term in the anisotropic part since it is much smaller. We attempted to fit a $TT_3(6,8)$ surface (see Ref. [25]) to the tabulated potential, but were unable to match the given dependence on the vibrational coordinate.

A new accurate *ab initio* potential surface expressed in terms of Legendre polynomials has been reported by Fu-Ming Tao [26] for intramolecular distances of 1.28, 1.449, and 1.618 a.u. This author claims that while the attractive region of the potential is adequately described by the first two terms (V_0 and V_2) of the potential, the next term, V_4 , may be needed to model accurately the highly repulsive region. The isotropic part of this potential is practically identical to the corresponding part of the Schaefer and Kohler potential [23]. Since it was more convenient to use the denser grid of the latter potential in our calculations, we have not pursued Tao's potential further.

A third *ab initio* potential has also recently appeared [27]. It has not been exploited since the results are not in a convenient form. However, the authors propose a functional form that may be faster to evaluate once it is decomposed into a series form as shown above. These authors note that the vibrational dependence or the derivative of the potential with respect to r changes sign twice. We have noted that the outer sign change ($R \cong 6.5$ a.u.) agrees well with the position of the sign change in the Schaefer and Meyer potential. Although the value of R at which the inner sign change occurs changes from approximately 2.0 for the Muchnick and Russek potential to 1.5 for the Schaefer and Meyer one, this is expected to be unimportant because this region of the potential is not probed by collisions. Even a head-on collision at an energy of 10^4 K in H_2 -He reaches only $R=3$ a.u.

B. Model and calculation

Line-shape parameters were calculated from the potential by using a standard semiclassical model [22]. The line shift and linewidth parameters for an optical transition $i \rightarrow f$ are given by [18,22,28]

$$\delta_{fi}(\text{cm}^{-1}) = \frac{n_b}{2\pi c} \langle v e^{-S_{2,fi}(b,v)} \sin \eta_{fi}(b,v) \rangle, \quad (9)$$

$$\gamma_{fi}(\text{cm}^{-1}) = \frac{n_b}{2\pi c} \langle v [1 - e^{-S_{2,fi}(b,v)} \cos \eta_{fi}(b,v)] \rangle,$$

where n_b is the number density of the perturbers and the symbol $\langle \dots \rangle$ means a Boltzmann average over the impact parameter b and the initial relative velocity v . The expression for $S_{2,fi}(b,v)$ is directly related to the real part of the differential cross section in the perturbation approach. That of $\eta_{fi}(b,v)$ is related to the first order and to the imaginary part of the second-order differential collision cross sections [cf. Eqs. (8) and (10) of Ref. [22]]. A parabolic trajectory based on the forces at the point of closest impact approximates the path of the colliding pair. In principle the model has two parts: the vibration-

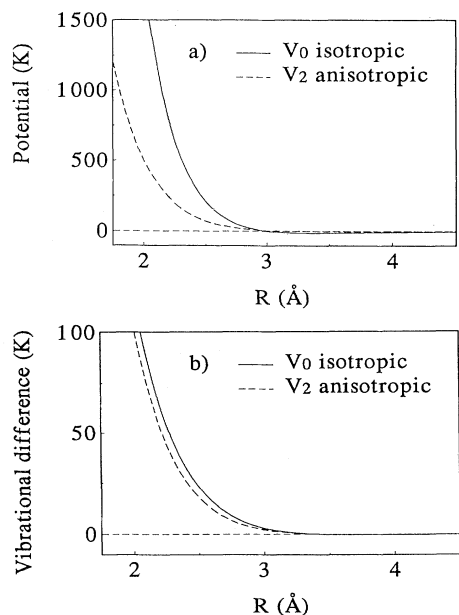


FIG. 7. Isotropic and anisotropic (P_2) parts of the potential: (a) in the $J=0, v=0$ state; (b) the difference between the potential in the $J=0, v=0$ and $J=0, v=1$ states.

al dephasing associated with the isotropic potential and the effect of the anisotropic potential leading to inelastic rotational transitions. The time integrals representing the effect of collisions were evaluated numerically. Test calculations with a Lennard-Jones parametrization of the potential which allowed analytic integration over time showed that the numeric approach was sufficiently accurate. The error bounds in the integrations were set at 0.1%.

The fact that inelastic collisions change the kinetic energy of the colliding pair leads to difficulties in describing the trajectory, especially for hydrogen since its rotational constant and the energy changes associated with rotational transitions are large. Consequently, an effective velocity v_{eff} equal to the arithmetic mean of the relative velocities before and after the collision was employed [$v_{\text{eff}} = (v_i + v_f)/2$]. Effective velocities were computed for elastic and inelastic collisions according to the algebraic change $h\nu$ in rotational state involved. The relative velocity satisfies the principle of conservation of energy,

$$\frac{1}{2}mv_i^2 = \frac{1}{2}mv_f^2 + h\nu. \quad (10)$$

This assumption [29] may appear crude at room temperature, but improves at higher temperatures: fewer molecules experience a large velocity change since their kinetic energy is much larger. This same calculation also allowed us to exclude inelastic collisions and especially upward ones that are forbidden due to the lack of sufficient kinetic energy. We also excluded collisions for which the effective velocity was small enough to permit metastable states ("orbiting"). This approximation introduces little error for the system since the potential well is small compared to the typical kinetic energies involved.

We note that only the isotropic part of the intermolecular potential is used to compute the trajectory. The first-order term in the theory, connected to elastic collisions, is computed from the vibrational dependence of the isotropic part of the potential. The anisotropic part is used in the calculation of the real part of the second-order term related to inelastic collisions. Finally, the imaginary part is found from the anisotropic potential and its dependence on the vibrational coordinate. Although it might be argued that the vibrational dephasing contribution associated with inelastic collisions [cf. Eq. (9)] should be calculated at the effective velocity v_{eff} [cf. Eq. (10)] for the inelastic collision, only a perturbative style of calculation allows such an approach. Trial calculations at 300 K, where the second-order terms are small

TABLE VII. Theoretical line-shift coefficients for H₂-He (expressed in $10^{-3} \text{ cm}^{-1} \text{ amagat}^{-1}$) at several temperatures.

J	296 K	596 K	795 K	995 K
0	7.4	12.4	14.9	17.0
1	7.9	13.7	16.7	19.3
2	8.1	14.3	17.6	20.3
3	8.2	14.8	18.3	21.3
4	8.3	15.0	18.7	21.9
5	8.2	15.0	18.8	22.2

TABLE VIII. Theoretical line broadening coefficients for H₂-He (expressed in $10^{-3} \text{ cm}^{-1} \text{ amagat}^{-1}$) at several temperatures.

J	296 K	596 K	795 K	995 K
0	1.3	4.4	6.8	9.4
1	0.8	2.1	3.3	4.7
2	1.2	2.8	4.1	5.5
3	1.1	2.6	3.7	4.9
4	0.9	2.2	3.2	4.2
5	0.9	2.0	2.8	3.6

enough to allow a series expansion without an Anderson-style cutoff [30], showed that the width of the $Q(0)$ line changes by 2% as a result of computing the vibrational part at the correct effective velocities. The linewidths of the remaining lines and all the shifts changed by less than 0.2%.

The imaginary terms from the first and second order

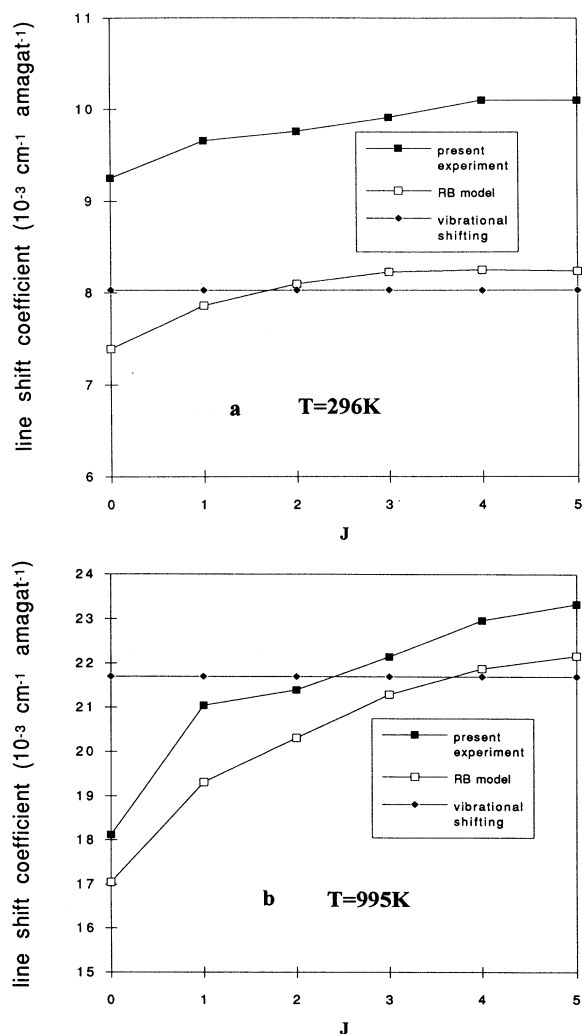


FIG. 8. Comparison between calculated (\square) and experimental (\blacksquare) line-shift coefficients for H₂-He: (a) at 296 K; (b) at 995 K [the theoretical pure vibrational dephasing contribution (\blacklozenge) is also shown].

TABLE IX. Pure dephasing contributions (expressed in 10^{-3} $\text{cm}^{-1} \text{ amagat}^{-1}$) calculated from Eq. (9) by only taking into account the isotropic potential.

T	296 K	596 K	795 K	995 K
δ_{deph}	8.0	14.6	18.3	21.7
γ_{deph}	0.8	1.6	2.1	2.7

lead to the line shift. The real terms act to reduce the magnitude of the shift cross section and to increase the width.

C. Results

Linewidths and line shifts were calculated at several temperatures for the six lowest rotational states and tabulated in Tables VII and VIII. Calculated shifts are in

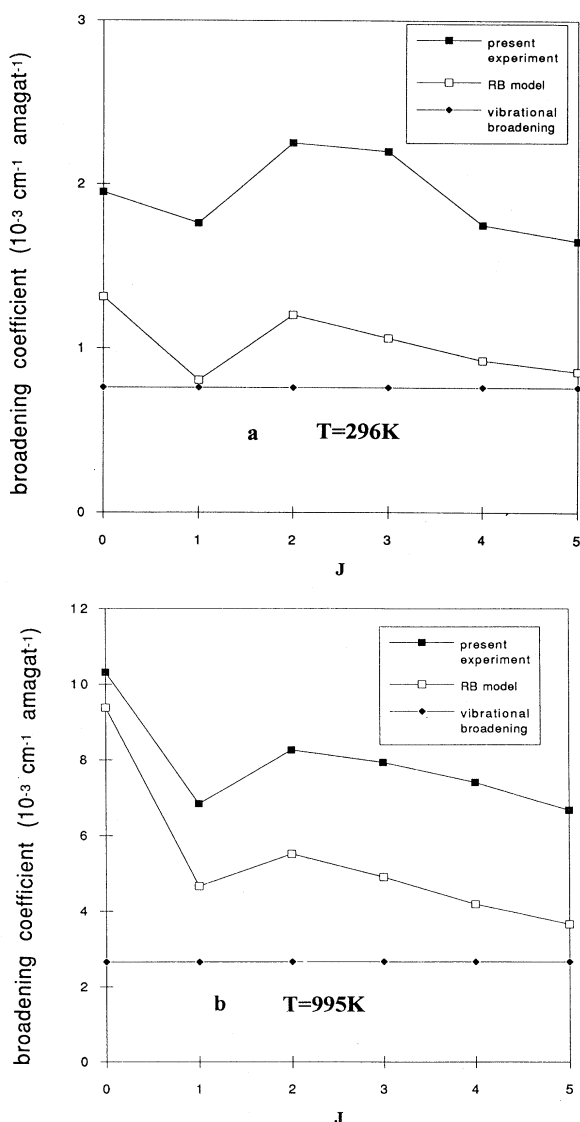


FIG. 9. Comparison between calculated and experimental line broadening coefficients for $\text{H}_2\text{-He}$. The symbols are the same as in Fig. 8.

very good agreement with experimental values (cf. Table II and Fig. 8). The difference in the line shifts is about 15% at 300 K and decreases to 5% at 995 K. We note that the theoretical results are based directly on the potential and that there are no adjustable parameters. The computed line broadening coefficients show a consistent description of the observed J and T dependence (cf. Table V), in spite of underestimating it by as much as 50% (cf. Table V and Fig. 9).

Additional calculations involving only the isotropic potential were performed in order to analyze the significance of the contributions of the different terms of the potential to the line shift and linewidth (Table IX). We found that the pure vibrational dephasing almost accounts for the observed line shift (cf. Table VII), but accounts for only half of the linewidth attributed to elastic dephasing in the analysis of the experimental data (cf. Table VI). The inelastic or second-order term introduces a J dependence in the results and helps to increase the calculated widths, but not enough to agree well with the experimental measurements. The imaginary second-order term has no significant effect for large J , due to the large rotational energy defect involved in the collisionally induced transitions. Only the $Q(0)$ and $Q(1)$ shifts show a weak decrease resulting from the contribution of the inelastic upward transitions $0 \rightarrow 2$ and $1 \rightarrow 3$, respectively. Notice that the screening effect, through the $S_{2,fi}(b, v)$ term in Eq. (9), is effective, particularly for the first line, which corresponds to the larger $S_{2,fi}(b, v)$ efficient contribution. This effect is of course more pronounced at higher temperature and reproduces well the observed J dependence (cf. Fig. 8).

The high probability of the inelastic $0 \rightarrow 2$ collisions, which nearly doubles the width at 300 K, explains the larger width of the $Q(0)$ line (cf. Table VIII and Fig. 9). The larger energy defect associated with the $1 \rightarrow 3$ transition increases the theoretical linewidth of the $Q(1)$ line by only 12% at 300 K (but 100% at 1000 K) over the vibrational dephasing. The higher $Q(J)$ lines are broader than the $Q(1)$ line since downward transitions are permitted, even if limited by detailed balance. The discrepancy in magnitude seems to result from an underestimation of the dephasing contribution. We have also noted that the theoretical inelastic terms fail to agree with the requirements of detailed balance. Such a problem is not surprising and is in part linked to the question of describing a classical trajectory involving an inelastic collision. Although the total transition rates to and from a state must be equal, it is assumed that these are dominated by transitions in which J changes only by ± 2 . An examination of the theoretical results shows that the upward rate is significantly larger than the corresponding downward rate for the same pair of states. The discrepancy decreases as the temperature increases or as the rotational energy gap decreases. Thus, aside from the previous discrepancy in the vibrational contribution, the $Q(0)$ and $Q(1)$ widths are likely to be overestimated because downward transitions are nonexistent. The other linewidths are probably underestimated since the dominant inelastic term is downward.

In spite of the interest for studying the $\text{H}_2\text{-He}$ system

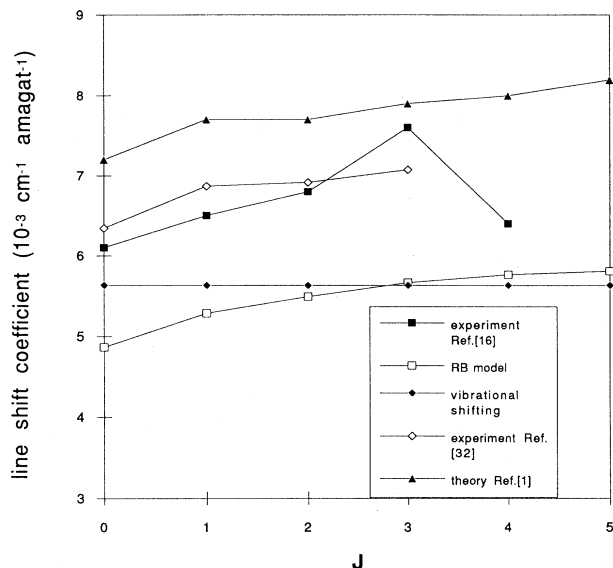


FIG. 10. Comparison between calculated (\square) and experimental [\blacksquare] Ref. [16]; (\diamond) Ref. [32]] line-shift coefficients for D₂-He at 296 K.

in both astronomy and chemical physics, very few *ab initio* calculations have been performed. Previous results of Hahne and Chackerian [31] using a close-coupling approach but a less accurate potential surface showed good agreement for the shift, but a poorer one for the broaden-

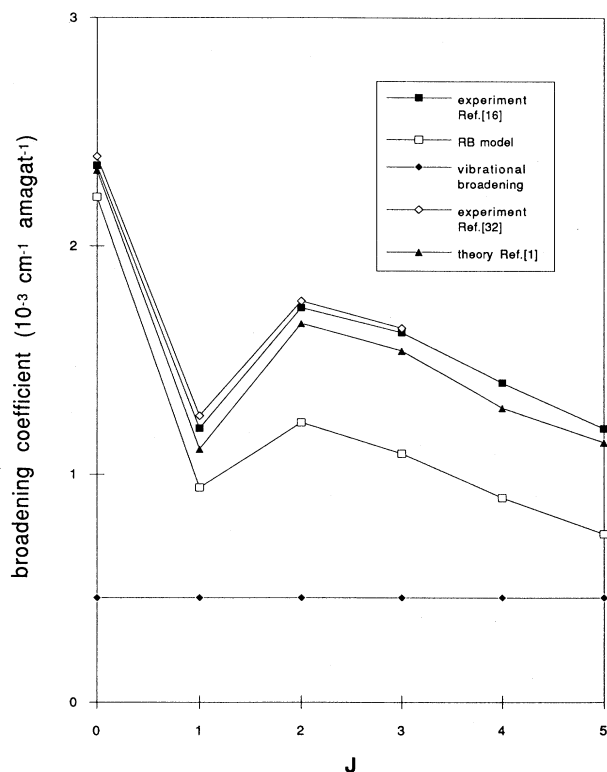


FIG. 11. Comparison between calculated (\square) and experimental [\blacksquare] Ref. [16]; (\diamond) Ref. [32]] line broadening coefficients for D₂-He at 296 K.

ing of the quadrupolar $Q_1(1)$ line. Direct comparison with the above results presents no real interest in the frame of this work since the potential surfaces used are different. So, in order to quantify the quality of the semiclassical results, calculations of the line shift and linewidth coefficients in D₂-He were compared with a fully quantum calculation [1] of linewidth and line-shift coefficients of the Q branch in D₂-He and experimental measurements in the D₂-He system [16,32]. Any differences between the two types of calculations are thus the result of the calculation, since the same *ab initio* potential was used. As in the H₂-He case, our semiclassical calculation underestimates the experimental results (Fig. 10), which were in good agreement with the quantum calculation. The pure vibrational contribution is again very predominant, particularly at high J . Comparison between quantum calculations [1] and semiclassical ones for the line broadening (Fig. 11) also shows a good consistency, although, as mentioned above for H₂-He, the pure dephasing contribution is underestimated. The agreement is better in that case since this last contribution is then weaker.

It appears that the semiclassical model is able to predict the J dependence (the inelastic part) of the widths and shifts even though there may be an error, especially for the width, in the elastic contribution from vibrational dephasing. Further semiclassical calculations for this contribution accounting for exact trajectories have been performed. The results are slightly improved but only by a few percent. So, any further rigorous test of the potential surface, particularly in the excited $v=1$ site, requires a fully quantum approach.

D. Temperature analysis

Apart from the above discussion concerning the J dependence of the line shifting and line broadening

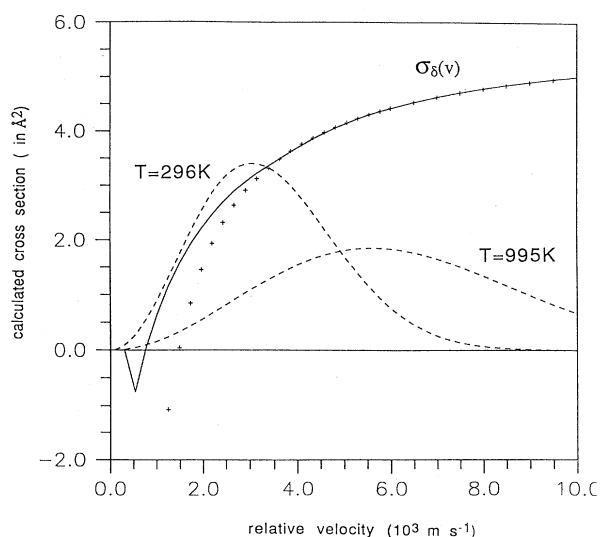


FIG. 12. Calculated shift cross sections $\sigma_\delta(v)$ (—) and least-squares fit (+) by the law: $\sigma_\delta(v) = 5.81 \text{ \AA}^2 - 8.45(\text{ \AA}^2 \cdot 10^3 \text{ m s}^{-1})/v$. The Boltzmann distribution is given at 296 and 995 K.

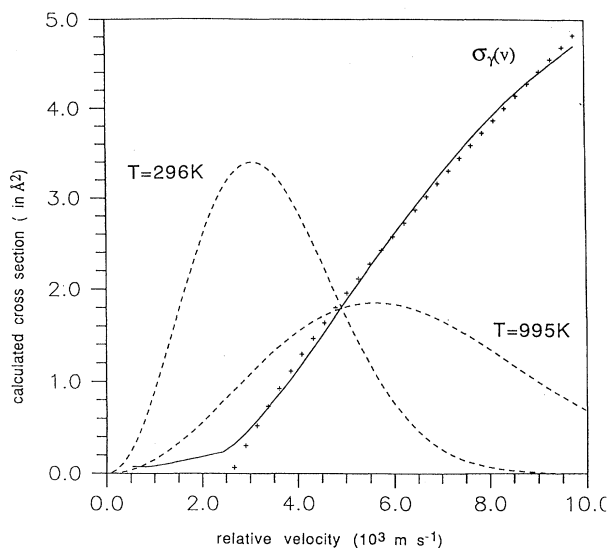


FIG. 13. Calculated broadening cross sections $\sigma_\gamma(v)$ (—) and least-squares fit (+) by the law: $\sigma_\gamma(v) = 0.53 (\text{\AA}^2 \cdot 10^{-3} \text{ m}^{-1} \text{ s}) v - 3.59 (\text{\AA}^2 \cdot 10^3 \text{ m s}^{-1})/v$. The Boltzmann distribution is given at 296 K and 995 K.

coefficients, the main result of these calculations is the remarkable consistency with the observed behavior: $\delta(T) = B\sqrt{T} + C$ and $\gamma(T) = A'T + C'$ (cf. Table III). So, interest lies in an analysis of the physical mechanisms underlying such simple laws.

For the line shift, since the pure vibrational mechanism is largely dominant, this analysis may be focused on it only. Figure 12 exhibits the expected behavior for the shift cross section $\sigma_\delta(v)$ in H_2 -He, since it is well described by $\sigma_\delta(v) = b + c/v$ (cf. Ref. [5]). In fact, such a simple v dependence is only valid for $v \gtrsim 3 \times 10^3 \text{ m s}^{-1}$, but the lowest values weakly contribute to the Boltzmann average of $v\sigma_\delta(v)$, even at room temperature. At high temperature, this model for $\sigma_\delta(v)$ becomes very accurate.

The inelastic rotational contribution being significant for $Q(0)$ and $Q(2)$ linewidths, the total broadening cross section $\sigma_\gamma(v)$ has been reported in Fig. 13 for the $Q(0)$ line as an example. The v dependence of this cross section is well approximated by $\sigma_\gamma(v) = a'v + c'/v$, particularly at high temperature, leading to the observed temperature variation.

Let us mention that similar behavior for these shift and width cross sections has been obtained previously from close-coupling calculation for D_2 -He (cf. Ref. [1]).

V. CONCLUSION

We have reported the line broadening and shifting coefficients of the Q branch in the H_2 -He system as a function of temperature and rotational state. The inelastic rates have been modeled with relaxation models. The ECS-P model and a simpler one, appropriate to H_2 , and based on considerations of detailed balance give good agreement with experiment. The contributions of vibrational dephasing and rotationally inelastic collisions have been deduced by using these models.

In a previous paper [5] devoted to other rare-gas perturbers, a significant inhomogeneous contribution to the line broadening due to the speed dependence of the line shift was demonstrated. No such evidence appears for H_2 -He, within experimental accuracy, but a possible inhomogeneous contribution remains plausible and has been carefully discussed.

Semiclassical calculations of the line shifts and linewidths based on the model of Ref. [22] and using an *ab initio* potential [23] have been performed from room temperature up to 995 K. The agreement is very good for the shifts, particularly at high temperature, allowing us to reproduce quantitatively the observed J and T dependences. For the widths, this agreement is less satisfactory, even if the J and T dependences are still accounted for. This discrepancy is attributed to an underestimation of the vibrational dephasing contribution. The possible residual inhomogeneous contribution to the observed widths has been estimated to be less than 20%, which is insufficient to explain such a discrepancy. Furthermore, the physical origin of the simple law observed for the temperature dependence of the shifts and the widths (i.e., linear versus $T^{1/2}$ and T , respectively) is well understood.

Of course, the present calculations are unable to test accurately the potential surfaces due to the approximations inherent to the semiclassical model used [22]. So, interest would lie in pure quantum calculations as previously done for D_2 -He in Ref. [1].

ACKNOWLEDGMENTS

The authors would like to thank CNES, CNRS, and SEP for financial support. The Laboratoire de Physique Moléculaire is URA CNRS No. 772, and the Laboratoire de Physique is URA CNRS No. 1796. One of the authors (J.W.F.) would like to acknowledge support from the Natural Sciences and Engineering Research Council of Canada.

- [1] R. Blackmore, S. Green, and L. Monchick, *J. Chem. Phys.* **88**, 4113 (1988); S. Green, R. Blackmore, and L. Monchick, *ibid.* **91**, 52 (1989).
 [2] L. A. Rahn, R. L. Farrow, and G. J. Rosasco, *Phys. Rev. A* **43**, 6075 (1991); L. A. Rahn and G. J. Rosasco, *ibid.* **41**, 3698 (1990).

- [3] R. L. Farrow, L. A. Rahn, and G. O. Sitz, *Phys. Rev. Lett.* **63**, 746 (1989).
 [4] D. Robert, J. M. Thuet, J. Bonamy, and S. Temkin, *Phys. Rev. A* **47**, R771 (1993).
 [5] J. Ph. Berger, R. Saint-Loup, H. Berger, J. Bonamy, and D. Robert, *Phys. Rev. A* **49**, 3396 (1994).

- [6] R. H. Dicke, *Phys. Rev.* **89**, 472 (1953).
- [7] P. Lallemand and P. Simova, *J. Mol. Spectrosc.* **26**, 262 (1968).
- [8] A. D. May, G. Varghese, J. C. Stryland, and H. L. Welsh, *Can. J. Phys.* **42**, 1058 (1964).
- [9] J. H. Dymond and E. B. Smith, *The Virial Coefficients of Pure Gases and Mixtures* (Clarendon, Oxford, 1980).
- [10] S. Perez, H. Smiedel, and B. Schramm, *Z. Phys. Chem.* **123**, 35 (1980).
- [11] J. Brewer and W. Vaughn, *J. Chem. Phys.* **50**, 2960 (1969).
- [12] J. O. Hirschfelder, C. F. Curtiss, and R. B. Bird, *Molecular Theory of Gases and Liquids* (Wiley, New York, 1964).
- [13] W. K. Bischel and M. J. Dyer, *Phys. Rev. A* **33**, 3113 (1986).
- [14] J. Bonamy and D. Robert, *Chem. Phys. Lett.* **57**, 22 (1978).
- [15] B. Lavorel, G. Millot, J. Bonamy, and D. Robert, *Chem. Phys.* **115**, 69 (1987).
- [16] K. C. Smyth, G. J. Rosasco, and W. S. Hurst, *J. Chem. Phys.* **87**, 1001 (1987).
- [17] A. E. De Pristo, S. D. Augustin, R. Ramaswamy, and H. Rabitz, *J. Chem. Phys.* **71**, 850 (1979).
- [18] L. Bonamy, J. Bonamy, D. Robert, B. Lavorel, R. Saint-Loup, R. Chauv, J. Santos, and H. Berger, *J. Chem. Phys.* **89**, 5568 (1988).
- [19] G. Millot, *J. Chem. Phys.* **93**, 8001 (1990).
- [20] W. Meier, G. Ahlers, and H. Zacharias, *J. Chem. Phys.* **85**, 2599 (1986).
- [21] K. Bratengeir, H. G. Purucker, and A. Laubereau, *Opt. Commun.* **70**, 393 (1989).
- [22] D. Robert and J. Bonamy, *J. Phys. (Paris)* **40**, 923 (1979).
- [23] J. Schaefer and W. E. Kohler, *Physica* **129A**, 469 (1985).
- [24] W. Meyer, P. C. Hariharan, and W. Kutzelnigg, *J. Chem. Phys.* **73**, 1880 (1980).
- [25] R. J. LeRoy and J. M. Hutson, *J. Chem. Phys.* **86**, 837 (1987).
- [26] Fu Ming Tao, *J. Chem. Phys.* **100**, 4947 (1994).
- [27] P. Muchnick and A. Russek, *J. Chem. Phys.* **100**, 4336 (1984).
- [28] J. Bonamy, D. Robert, and C. Boulet, *J. Quantum Spectrosc. Radiat. Transfer* **31**, 23 (1984).
- [29] G. D. Billing, *Chem. Phys. Lett.* **50**, 320 (1977).
- [30] P. W. Anderson, *Phys. Rev.* **76**, 647 (1949); C. J. Tsao and B. Curnutte, *J. Quantum Spectrosc. Radiat. Transfer* **2**, 41 (1962).
- [31] G. E. Hahne and C. Chackerian, *J. Chem. Phys.* **73**, 3223 (1980).
- [32] P. M. Sinclair, P. Duggan, M. Le Flohic, J. W. Forsman, J. R. Drummond, and A. D. May, *Can. J. Phys.* **72**, 885 (1994).